nature portfolio

https://doi.org/10.1038/s41562-021-01218-1

Supplementary information

Origins and spread of formal ceremonial complexes in the Olmec and Maya regions revealed by airborne lidar

In the format provided by the authors and unedited

Supplementary Information

Supplementary Discussion 1: Effectiveness of the INEGI lidar

Here we present additional information on the effectiveness of the INEGI lidar and the effects of vegetation on the INEGI lidar. The INEGI lidar has low data densities, whereas the NCALM and G-LiTH lidars have higher data densities (Supplementary Table 1). Supplementary Fig. 1 demonstrates how different types of INEGI lidar visualization show archaeological features and are affected by vegetation. They include original INEGI DEMs (5 m horizontal resolution), INEGI DSMs (5 m horizontal resolution), reprocessed INEGI DEMs (2 m horizontal resolution), and Red Relief Image Maps (RRIMs) based on the 5 m-resolution DEMs. Supplementary Table 2 shows estimates of vegetation types based on the INEGI lidar by areas of different lidar coverages.

The original INEGI DEMs show many archaeological features in areas of sparse vegetation, but their function is more limited in areas of dense vegetation. In some cases, structures are filtered out in the original DEMs. DSMs may show such features better. Many of those features that were filtered out in the original DEMs became visible in the reprocessed DEMs. Red Relief Image Maps (RRIMs) enhance the visibility of subtle features. Supplementary Table 3 shows the detection accuracies and error rates by types of archaeological complex and lidar coverage.

Supplementary Table 1 │ Summary of the lidar data examined in this study.

Lidar	Area within the study area (km^2)	Data acquisition date	Lidar	Aircraft	Flight height above ground level (m)	Pulse repetition frequency (kHz)	Scan frequency (Hz)	Scan angle (degree)	Swath width (m)	Swath overlap (%)	Pulse density (/m^2)	Return density (/m^2)	Ground return density (/m^2)	DEM horizontal resolution (m)
NCALM	1,015	May, 2017; June, 2019	Optech Titan	Piper PA-31-350 Navajo Chieftain	650	450 (3 channels with 150 each)	25.0	60	750	50	14.7	18.5	10.4	1 (2017 data) and 0.5 (2019 data)
INEGI	84,516	2007, 2008 and 2009	Leica ALS50-II	Cessna 441 Conquest II	5,000 to 5,800	20.6	9.1	60	6750	20	0.0368	0.0370	0.0285	5 (INEGI DEM) and 2 (reprocessed DEM)
NASA G-LiHT	99	April-May, 2013	Riegl VQ-480	Piper Cherokee, N4118R	335	300.0		60	400	0	5.6	8.1	4.8	1
CCGS	10										10.1	19.4	1.9	0.5

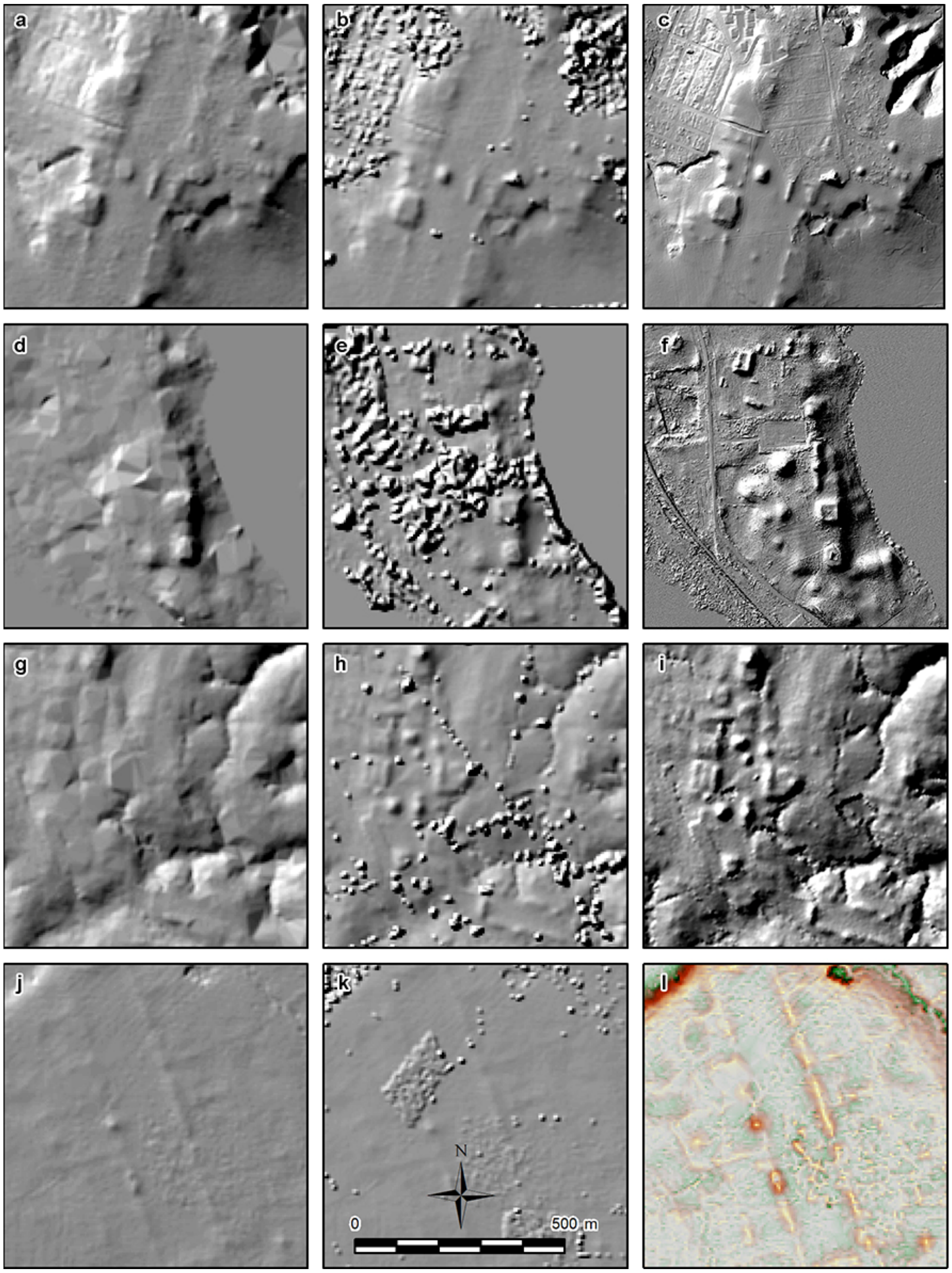

Supplementary Figure 1 | Comparison of INEGI DEM, INEGI DSM, NCALM DEM and RRIM.

a-c, La Carmelita. In this area of pasture, the INEGI DEM shows small mounds fairly well. **a,** 5 m INEGI DEM. **b,** 5 m INEGI DSM. **c,** 1 m NCALM DEM. **d-f,** El Tiradero. In forested parts, the INEGI lidar does not show archaeological features well. **d,** 5 m INEGI DEM. **e,** 5 m INEGI DSM. **f,** 0.5 m NCALM DEM. **g-i,** Kilómetro 15. In some cases, structures are filtered out in INEGI DEMs, and DSMs can be more useful in identifying archaeological features. The reprocessed INEGI lidar data shows significant improvement. **g,** 5 m INEGI DEM. **h,** 5 m INEGI DSM. **i,** Reprocessed 2 m DEM. **j-l,** Aguapinde. The RRIM visualization technique enhances the visibility of subtle features. **j,** Hillshade of 5 m INEGI DEM. **k,** Hillshade of 5 m INEGI DSM. **l,** RRIM of 5 m INEGI DEM. All images are on the same scale.

Supplementary Table 2 | Pixel counts by vegetation heights and lidar coverage according to the Canopy Height Model (CHM) at a horizontal resolution of 5 m derived from the INEGI lidar.

	Canopy height										
Lidar	0-0.5 m		0.5-1.5 m		1.5-3.5 m		3.5-15 m		15-60 m		Total
coverage	Count	%	Count	%	Count	%	Count	%	Count	%	
NCALM1	2,124,425	74.0	181,401	6.3	181,171	6.3	355,994	12.4	26,117	0.9	2,869,108
NCALM2	4,530,826	62.9	656,737	9.1	747,313	10.4	1,246,397	17.3	19,502	0.3	7,200,775
NCALM3	8,344,988	69.8	1,014,545	8.5	934,002	7.8	1,599,019	13.4	56,679	0.5	11,949,233
NCALM4	6,780,541	75.9	549,150	6.1	501,153	5.6	1,025,045	11.5	82,224	0.9	8,938,113
NCALM5	3,057,055	68.9	311,259	7.0	306,214	6.9	715,567	16.1	45,400	1.0	4,435,495
NCALM6	535,597	81.0	41,542	6.3	42,271	6.4	42,001	6.3	140	0.0	661,551
NCALM7	626,316	75.6	50,574	6.1	51,228	6.2	97,834	11.8	2,168	0.3	828,120
NCALM8	2,704,451	72.5	332,193	8.9	257,536	6.9	403,847	10.8	31,600	0.8	3,729,627
G-LiHT1	23,256	9.2	10,810	4.3	22,254	8.8	148,334	59.0	46,859	18.6	251,513
G-LiHT2	842,075	60.4	114,851	8.2	135,288	9.7	268,947	19.3	33,368	2.4	1,394,529
G-LiHT3	130,712	51.4	21,177	8.3	28,899	11.4	65,380	25.7	8,321	3.3	254,489
G-LiHT4	80,466	65.0	9,347	7.6	9,493	7.7	22,578	18.2	1,864	1.5	123,748
G-LiHT5	422,930	53.7	68,227	8.7	88,410	11.2	202,970	25.8	4,647	0.6	787,184
G-LiHT6	316,154	28.1	137,181	12.2	170,092	15.1	482,805	42.8	20,808	1.8	1,127,040
CCGS	98811	25.9	22759	6.0	45290	11.9	198410	51.9	16901	4.4	382,171
Total high-resolution lidar areas	30,618,603	68.1	3,521,753	7.8	3,520,614	7.8	6,875,128	15.3	396,598	0.9	44,932,696
Area covered only by INEGI	2,025,741,643	60.7	288,558,222	8.7	311,127,304	9.3	619,637,720	18.6	90,177,930	2.7	3,335,242,819
All area	2,056,360,246	60.8	292,079,975	8.6	314,647,918	9.3	626,512,848	18.5	90,574,528	2.7	3,380,175,515

G-LiHT Transect 5, which goes through the Campeche hills and nearby areas, also helps us understand the effect of vegetation on the INEGI lidar (Supplementary Fig. 2). The lower elevation zone includes seasonal and permanent wetlands, where patches of dense vegetation are present, but mound densities are low. In the lower slope zone, mound densities are high, and vegetation is patchy. In areas of sparse vegetation, mounds are visible in the INEGI lidar, but those covered by dense vegetation are not detected in the INEGI lidar. In the Campeche hills, mound densities appear to decrease as the distance from the lower slope zone increases. Many mounds are not visible in the INEGI lidar because of dense vegetation.

These data suggest that the Campeche hills, along with the Palenque-Chinikiha zone of the Chiapas Mountains, are particularly problematic areas (Fig. 1c). The distribution of mound groups in those areas needs to be examined with higher-resolution lidar in the future. In areas of patchy vegetation, the detection rate of mound groups varies depending on the distribution of vegetation patches. We should add that those observations specifically concern minor mound groups that do not fit into the categories of standardized ceremonial complexes or major and minor centres. Many of those mound groups probably date to the Classic period. The distribution and the detection patterns of larger Formative complexes are different. It is unlikely that there are many larger Formative complexes in the rugged terrains of the Campeche hills and the Palenque-Chinikiha zone because those complexes are invariably found in flat terrains. In addition, major Formative complexes often have horizontal dimensions larger than patches of vegetation. Thus, many of them are identifiable in areas of patchy vegetations. Supplementary Table 3 shows that the detection rate of smaller Formative complexes is lower than those of larger complexes but generally higher than those of minor mound groups.

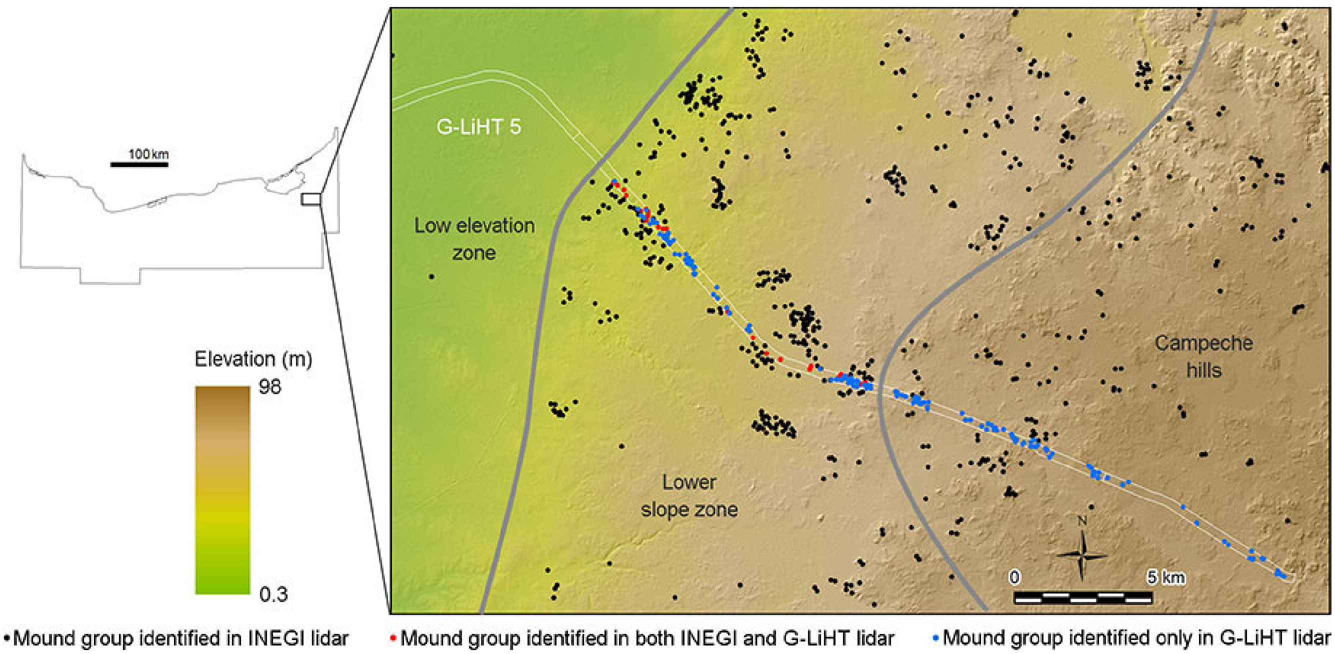

Supplementary Figure 2 | Close-up of G-LiHT Transect 5.

The map shows the different zones of topographic and vegetation conditions and the distribution of mound groups.

Supplementary Table 3 | Archaeological complexes and mound groups identified in lidar data.

The detection accuracies and error rates are indicated by types of archaeological complex and lidar coverage. Overall accuracy = positive verification / (positive verification + addition from high-res lidar). Commission error = discarded / (positive verification + discarded). Omission error = Addition from high-res lidar / (positive verification + addition from high-res lidar).

			High-resolution lidar				Accuracy		
Lidar coverage	IDed in INEGI	Added from literature	Positive verification	Discarded	Addition from high-res lidar	Total ID in high-res lidar	Overall accuracy (%)	Commission error (%)	Omission error (%)
NCALM 1									
MFU	2		2			2	100.0		
Centre major	5		5			5	100.0		
Centre minor	5		5			5	100.0		
Rectangle minor	1		1			1	100.0		
Mound group	309		307	2	224	531	57.8	0.6	42.2
Subtotal	322		320	2	224	544	58.8	0.6	41.2
NCALM 2									
MFU					1	1	0.0		100.0
MFU minor	4		4		6	10	40.0		60.0
MFC	1		1			1	100.0		
E Group	1		1			1	100.0		
Centre major	3		3		1	4	75.0		25.0
Centre minor	9		9		9	18	50.0		50.0
Rectangle minor	5		5		1	6	83.3		16.7
Square					4	4	0.0		100.0
Mound group	430		430		748	1,178	36.5		63.5
Subtotal	453		453		770	1,223	37.0		63.0
NCALM 3									
MFU primary	1		1			1	100.0		
MFU	2		2			2	100.0		
MFU minor	11		11		9	20	55.0		45.0
MFC	1		1			1	100.0		
Centre major	4		4		1	5	80.0		20.0
Centre minor	19		19		14	33	57.6		42.4
Rectangle major	4		4			4	100.0		
Rectangle minor	28		28		22	50	56.0		44.0
Square	1		1		2	3	33.3		66.7
Mound group	463		463		1,995	2,458	18.8		81.2
Subtotal	534		534		2,043	2,577	20.7		79.3

Supplementary Table 3 (Continued)

Lidar coverage	IDed in INEGI	Added from literature	High-resolution lidar: Positive verification	High-resolution lidar: Discarded	High-resolution lidar: Addition from high-res lidar	High-resolution lidar: Total ID in high-res lidar	Accuracy: Overall accuracy (%)	Accuracy: Commission error (%)	Accuracy: Omission error (%)
NCALM 4									
MFU	5		5			5	100.0		
MFU minor	10		10		5	15	66.7		33.3
Centre primary	1		1			1	100.0		
Centre major	4		4		1	5	80.0		
Centre minor	9		9		2	11	81.8		18.2
Rectangle major	2		2		2	4	50.0		50.0
Rectangle minor	10		10		9	19	52.6		47.4
Square	9		9		6	15	60.0		40.0
Mound group	355		354	1	451	805	44.0	0.3	56.0
Subtotal	405		404	1	476	880	45.9	0.2	54.1
NCALM 5									
MFU minor	2		2		1	3	66.7		33.3
Centre major	3		3			3	100.0		
Centre minor	6		6		3	9	66.7		33.3
Rectangle major	2		2			2	100.0		
Rectangle minor	3		3		2	5	60.0		40.0
Mound group	354		346	8	1,157	1,503	23.0	2.3	77.0
Subtotal	370		362	8	1,163	1,525	23.7	2.2	76.3
NCALM 6									
MFC	1		1			1	100.0		
Rectangle minor	6		6		1	7	85.7		14.3
Mound group	81		78	3	94	172	45.3	3.7	54.7
Subtotal	88		85	3	95	180	47.2	3.4	52.8
NCALM 7									
Centre minor	2		2			2	100.0		
Mound group	16		14	2	39	53	26.4	12.5	73.6
Subtotal	18		16	2	39	55	29.1	11.1	70.9
NCALM 8									
MFU	1		1			1	100.0		
Centre major	1		1			1	100.0		
Centre minor	1		1			1	100.0		
Rectangle minor	1		1			1	100.0		
Mound group	45	1	45		103	148	30.4		69.6
Subtotal	49	1	49		103	152	32.2		67.8

Supplementary Table 3 (Continued)

Lidar coverage	IDed in INEGI	Added from literature	High-resolution lidar: Positive verification	Discarded	Addition from high-res lidar	Total ID in high-res lidar	Accuracy: Overall accuracy (%)	Commission error (%)	Omission error (%)
G-LiHT 1									
Mound group					4	4	0.0		100.0
Subtotal					4	4	0.0		100.0
G-LiHT 2									
Mound group	5			5	8	8	0.0	100.0	100.0
Subtotal	5			5	8	8	0.0	100.0	100.0
G-LiHT 3									
Mound group					15	15	0.0		100.0
Subtotal					15	15	0.0		100.0
G-LiHT 4									
Subtotal									
G-LiHT 5									
Centre minor	1		1			1	100.0		
Mound group	23		23		157	180	12.8		87.2
Subtotal	24		24		157	181	13.3		86.7
G-LiHT 6									
Centre minor					1	1			100.0
Mound group	5		4	1	324	328	1.2	20.0	98.8
Subtotal	5		4	1	325	329	1.2	20.0	98.8
CCGS									
Subtotal									

Summary for high-resolution lidar areas	IDed in INEGI	Added from literature	Positive verification	Discarded	Addition from high-res lidar	Total ID in high-res lidar	Overall accuracy (%)	Commission error (%)	Omission error (%)
MFU primary	1		1			1	100.0		
MFU	10		10		1	11	90.9		9.1
MFU minor	27		27		21	48	56.3		43.8
MFC	3		3			3	100.0		
E Group	1		1			1	100.0		
Centre primary	1		1			1	100.0		
Centre major	20		20		3	23	87.0		13.0
Centre minor	52		52		29	81	64.2		35.8
Rectangle major	8		8		2	10	80.0		20.0
Rectangle minor	54		54		35	89	60.7		39.3
Square	10		10		12	22	45.5		54.5
Mound group	2,086	1	2,064	22	5,319	7,383	28.0	1.1	72.0
Total	**2,273**	**1**	**2,251**	**22**	**5,422**	**7,673**	**29.3**	**1.0**	**70.7**

Supplementary Table 3 (Continued)

INEGI only (outside the high-resolution lidar areas)

	IDed in INEGI	Added from literature	Total
MFU	36		36
MFU minor	27		27
MFC	8		8
MFG primary	1		1
MFG	3		3
VC	29		29
VC minor	7		7
E Group	2		2
Centre primary	8	1	9
Centre major	60	2	62
Centre minor	228	14	242
Classic Veracruz major	100	1	101
Classic Veracruz minor	201	1	202
Classic Veracruz minimal	65		65
Rectangle major	60		60
Rectangle minor	116		116
Rectangle minimal	49		49
Square	7		7
Mound group	25,235		25,235
Total	**26,242**	**19**	**26,261**

Supplementary Table 3 (Continued)

Entire study area

	IDed in INEGI	Added from literature	Discarded	Addition from high-res lidar	Total (INEGI + literature + high res - discarded)
MFU primary	1				1
MFU	46			1	47
MFU minor	54			21	75
MFC	11				11
MFG primary	1				1
MFG	3				3
VC	29				29
VC minor	7				7
E Group	3				3
Centre primary	9	1			10
Centre major	80	2		3	85
Centre minor	280	14		29	323
Classic Veracruz major	100	1			101
Classic Veracruz minor	201	1			202
Classic Veracruz minimal	65				65
Rectangle major	68			2	70
Rectangle minor	170			35	205
Rectangle minimal	49				49
Square	17			12	29
Mound group	27,321	1	22	5,319	32,619
Total	**28,515**	**20**	**22**	**5,422**	**33,935**

Supplementary Table 4 | Summary of site types.

Type	Definition	Date estimate
Middle Formative Usumacinta (MFU) pattern	Rectangular formation defined by rows of low mounds; E Group in the centre; some E Groups have two pyramids on the western side; a cache containing greenstone axes and other objects was found along the east-west axis of the E Group at Aguada Fénix. Subdivided into primary MFU, MFU and minor MFU. Primary MFU = the largest (Aguada Fénix) MFU: length >= 400 m Minor MFU: length < 400 m	Early half of the Middle Formative, but some may have started toward the end of the Early Formative
Veracruz ceremonial (VC) pattern	Rectangular formation defined by rows of low mounds or continuous linear mounds; some have an E Group, but others do not; a wing defined by rows of low mounds or continuous linear mounds attached to the rectangle, usually on the west side. Subdivided into VC and minor VC. VC: length >= 400 m Minor VC: length < 400 m	Probably the early half of the Middle Formative, but some may be Early Formative
Middle Formative Chiapas (MFC) pattern	E Group; large platforms placed along the north-south axis of the E Group; some have a north pyramid; caches containing greenstone axes and other offerings were found along the east-west axis of the E Group at San Isidro, Chiapa de Corzo and Ceibal.	Mostly Middle Formative, but some date to the Late and Terminal Formative
Middle Formative Gulf (MFG) pattern	This is a sub-type of the MFC pattern: E Group and a north pyramid; side platforms are placed close to each other, forming straight lines along the plaza; caches containing greenstone axes and other offerings were found in an area north of the north pyramid at La Venta. Subdivided into primary MFG and MFG. Primary MFG: the largest (La Venta) MFG: other than La Venta	Probably Middle Formative
Rectangular complex	Rectangular formation defined by rows of low mounds or continuous linear mounds, similar to the MFU but without an E Group. Subdivided into major, minor and minimal types. Major: length >= 400 m Minor: length < 400 m, usually > 100 m Minimal: length mostly < 150 m; defined by continuous linear mounds	Most of the major and minor rectangular complexes probably date to the early part of the Middle Formative; some minimal rectangular complexes may date to later periods.
Square complex	Square formation defined mostly by continuous linear mounds; some have a single mound in the centre, but others do not.	Early part of the Middle Formative?

Supplementary Table 4 (continued)

Classic Veracruz pattern	These complexes have also been called the Standard Plan, Long-Plaza Plan, Villa Alta Quadripartite Arrangement, or Tipo 4. They have a plaza defined by linear lateral platforms; they have either a pyramid on each of the two ends or a pyramid on one end and a lower mound on the other. Subdivided into the major, minor and minimal types. The classification is arbitrary, based on the sizes of individual mounds, the overall size of the complex and surrounding buildings, and the number of mounds. Major: length > 100 m; taller end pyramid > 9.7 m; they may have other Classic Veracruz complexes or other substantial constructions nearby. Minor: length < 185 m, > 70 m; taller end pyramid < 12 m, > 0.5 m; They may have medium-sized buildings around it and a moderate number of mounds. Minimal: length < 110 m; taller end pyramid < 10 m; no other substantial constructions around it.	Late and Terminal Classic
Centre	Complexes including substantial buildings, which probably had administrative or ceremonial functions; do not fit the categories of the MFU, VC, MFC, MFG, rectangular complex, or Classic Veracruz pattern. Subdivided into primary, major and minor types. The classification is arbitrary, based on the sizes of individual mounds, the overall size of the central complex and the number of mounds. Primary: Important administrative centres, including San Lorenzo, Laguna de los Cerros, Tres Zapotes, Matacapan, Palenque, Pomona, Moral-Reforma, El Tortuguero, El Tigre and Comalcalco. Major: Tallest structure > 3.5 m (> 6 m in many cases); large overall size Minor: Tallest structure < 11.5 m (< 8 m in many cases); small overall size	Include Formative centres, such as San Lorenzo, Laguna de los Cerros and Tres Zapotes; most of them date to the Late Formative to Postclassic; in many cases, the main occupation is likely Classic.
Mound group	Spatial aggregation of multiple mounds of moderate to small sizes, but isolated single mounds are also included; most of them are assumed to be residential groups; some are patio groups with multiple mounds surrounding a patio, and others have irregular forms. Because the study area includes diverse forms of archaeological features, the identification of mound groups remained flexible and arbitrary.	Most of them probably date to the Late Formative to Postclassic; in many cases, the main occupation is likely Classic.

Supplementary Discussion 2: Locational data

The GIS database of all sites identified in this study is made publicly available at the University of Arizona Campus Repository (https://repository.arizona.edu/handle/10150/635527). The publication of the locational data of archaeological sites requires careful evaluations because such information may lead to an increase in looting. In the case of our study area, we judged that the benefit of publication is significantly larger than its potentially detrimental effects. The INEGI lidar data, which is the primary basis of our identification of archaeological sites, are already publicly available. In addition, a substantial part of our study region is deforested and used as ranches, orchards and agricultural fields. In most cases, local people probably know about mounded sites that are in their areas. Many of those sites, however, were not known to archaeologists before this study. This dataset allows archaeologists to study these sites efficiently and help the Mexican government to develop a plan to better protect them.

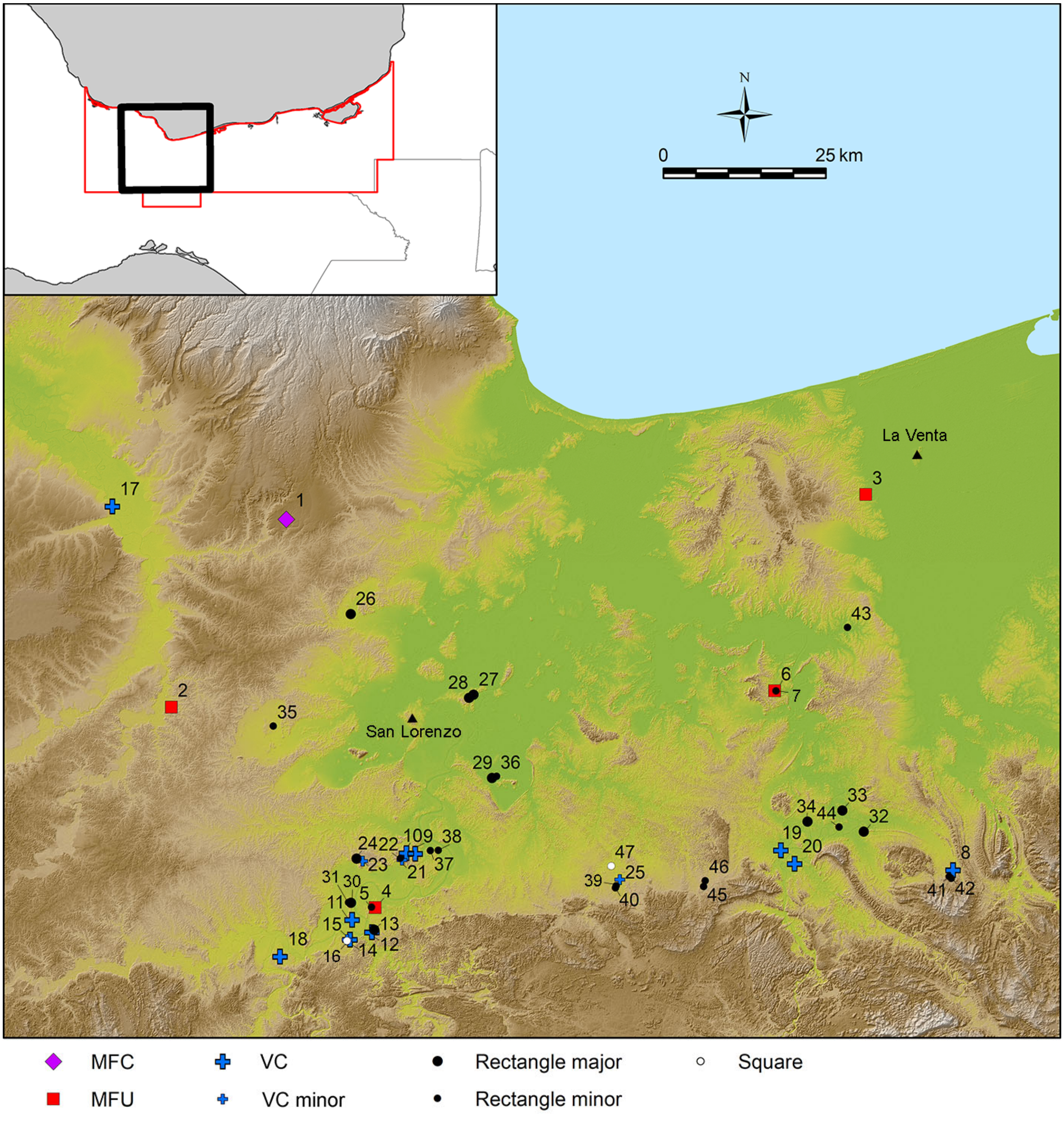

Supplementary Figure 3 | Formative complexes in southern Veracruz investigated during the INAH survey.
The numbers correspond to those in Supplementary Table 5.

Supplementary Table 5 | Formative complexes in southern Veracruz investigated during the INAH survey.
The numbers in the location column correspond to those in Supplementary Fig. 3.

Location	Name	INAH site code	Type	Map	Surface-collected ceramics
1	El Hato	050AL2D	MFC	MFC mapped	Late Classic
2	Achotal-Gravera	126AL2D	MFU	Originally classified as a major centre in the lidar analysis. INAH mapped an MFU-MFG-like configuration.	Formative (Early Formative)
3	La Duda	039TPS	MFU	MFU not mapped besides the E Group	Formative, Classic, Postclassic
4	El Zapotal	074CH	MFU	MFU not mapped	Formative
5	El Zapotal	074CH	Rectangle minor	Rectangle partially mapped	Formative
6	Viva la Revolución II	234TPS	MFU	MFU not mapped besides the E Group east mound	
7	Viva la Revolución II	234TPS	Rectangle minor	Rectangle partially mapped	
8	Arroyo el Pedregal	039TPS-N	VC	Rectangle not mapped	Late Classic
9	Rancho la Estrella	059CH	VC	VC not mapped besides wing mounds	Formative (Early Formative)
10	Rancho la Estrella	059CH	VC	VC partially mapped	Formative (Early Formative)
11	La Oaxaqueña	087CH	VC	VC not mapped	Formative (Early Formative)
12	Boca de Chalchijapan	092CH	VC	VC mapped, but not its form not well recognized	Formative (Early Formative and probable Middle Formative), Late Classic
13	Boca de Chalchijapan	092CH	Rectangle major	Rectangle mapped	Formative (Early Formative and probable Middle Formative), Late Classic
14	Río Abundancia	093CH	VC	VC partially mapped	
15	Río Abundancia	093CH	VC minor	Main rectangle of VC mapped, but not the west wing	
16	Río Abundancia	093CH	Square	Square partially mapped	
17	El Marquesillo		VC?	Salvage excavation by INAH	Formative (Early and Middle Formative), Classic

Supplementary Table 5 (Continued)

Location	Name	INAH site code	Type	Map	Surface-collected ceramics
18	Suchilapan del Río I	013SS	VC	Originally not classified as an VC in the lidar analysis as it appeared to be a modern construction. Mapped as an archaeological site by INAH.	
19	El Mirador de Francisco	424TPS	VC	VC partially mapped	Formative, Late Classic
20	San Miguel	425TPS	VC	West wing of VC mapped, but not the main rectangle	Formative
21	San Marcos	061CH	VC minor	VC partially mapped	Formative, Late Classic
22	San Marcos	061CH	Rectangle minor	Rectangle not mapped	Formative, Late Classic
23	Colonia Ojo de Agua III	065CH	VC minor	VC not mapped	Formative (Early Formative)
24	Colonia Ojo de Agua III	065CH	Rectangle major	Rectangle not mapped	Formative (Early Formative)
25	20 de Noviembre el Romay	063CHS	VC minor	VC not mapped besides wing mounds	Late Classic
26	Rancho San Juan	081AL2D	Rectangle major	Rectangle not mapped	
27	Rancho la Gloria Ahuatepec	004CH	Rectangle major	Rectangle not mapped	Formative, Late Classic
28	Rancho la Gloria Ahuatepec	004CH	Rectangle major	Rectangle partially mapped	Formative, Late Classic
29	El Macayal	014CH	Rectangle major	Rectangle not mapped	Formative
30	El Edén	073CH	Rectangle major	Rectangle not mapped	Formative
31	El Edén	073CH	Rectangle minor	Rectangle not mapped	Formative
32	La Techcalera	048TPS	Rectangle major	Rectangle partially mapped	
33	El Zapote	104TPS	Rectangle major	Rectangle not mapped	Formative, Late Classic, Late Postclassic

Supplementary Table 5 (Continued)

Loca-tion	Name	INAH site code	Type	Map	Surface-collected ceramics
34	Rancho Adalberto Tejeda	317TPS	Rectangle major	Rectangle partially mapped	Formative, Late Classic, Late Postclassic
35	El Juile I	121AL2D	Rectangle minor	Rectangle not mapped	Formative, Late Classic
36	Isla el Macayal	013CH	Rectangle minor	Rectangle mapped	Formative
37	Laguna Grande II	056CH	Rectangle minor	Rectangle not mapped	Formative, Late Classic
38	Laguna Grande II	056CH	Rectangle minor	Rectangle mapped, may not be a Formative complex	Formative, Late Classic
39	Los Pavorreales	064CHS	Rectangle minor	Rectangle mapped	Formative, Late Classic
40	Los Pavorreales	064CHS	Rectangle minor	Rectangle mapped	Formative, Late Classic
41	Los Callejas	041TPS	Rectangle minor	Rectangle mapped	Formative, Late Classic, Late Postclassic
42	Los Callejas	041TPS	Rectangle minor	Rectangle partially mapped	Formative, Late Classic, Late Postclassic
43	Heriberto Carrillo	182TPS	Rectangle minor	Rectangle not mapped	Formative, Classic
44	Los Morritos	312TPS	Rectangle minor	Rectangle partially mapped	Formative, Late Classic, Late Postclassic
45	Reforma-Carolino Anaya	390TPS	Rectangle minor	Rectangle mapped	Late Classic
46	Reforma-Carolino Anaya	390TPS	Rectangle minor	Rectangle partially mapped	Late Classic
47	Gral. S. Taboada II Los Juanes	060CHS	Square	Square not mapped	Late Classic

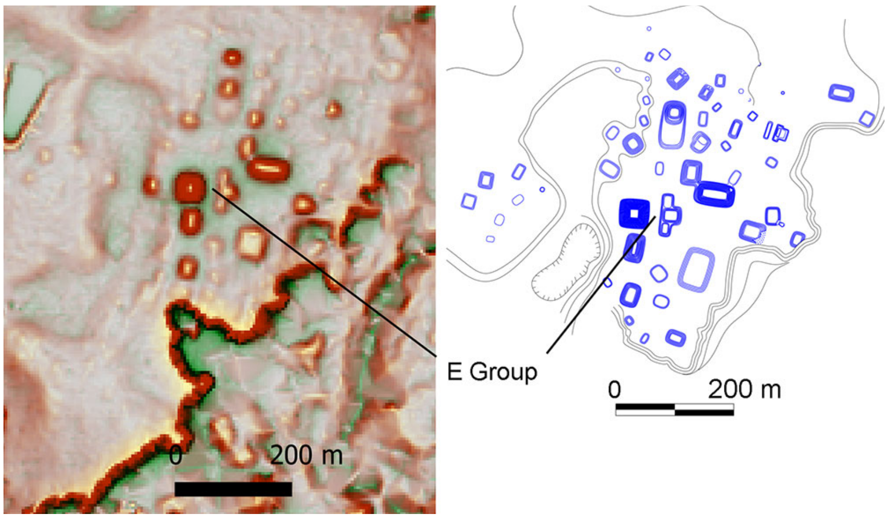

Supplementary Figure 4 │ El Hato.

The MFC complex is visible both in the lidar-derived RRIM and in the INAH map.

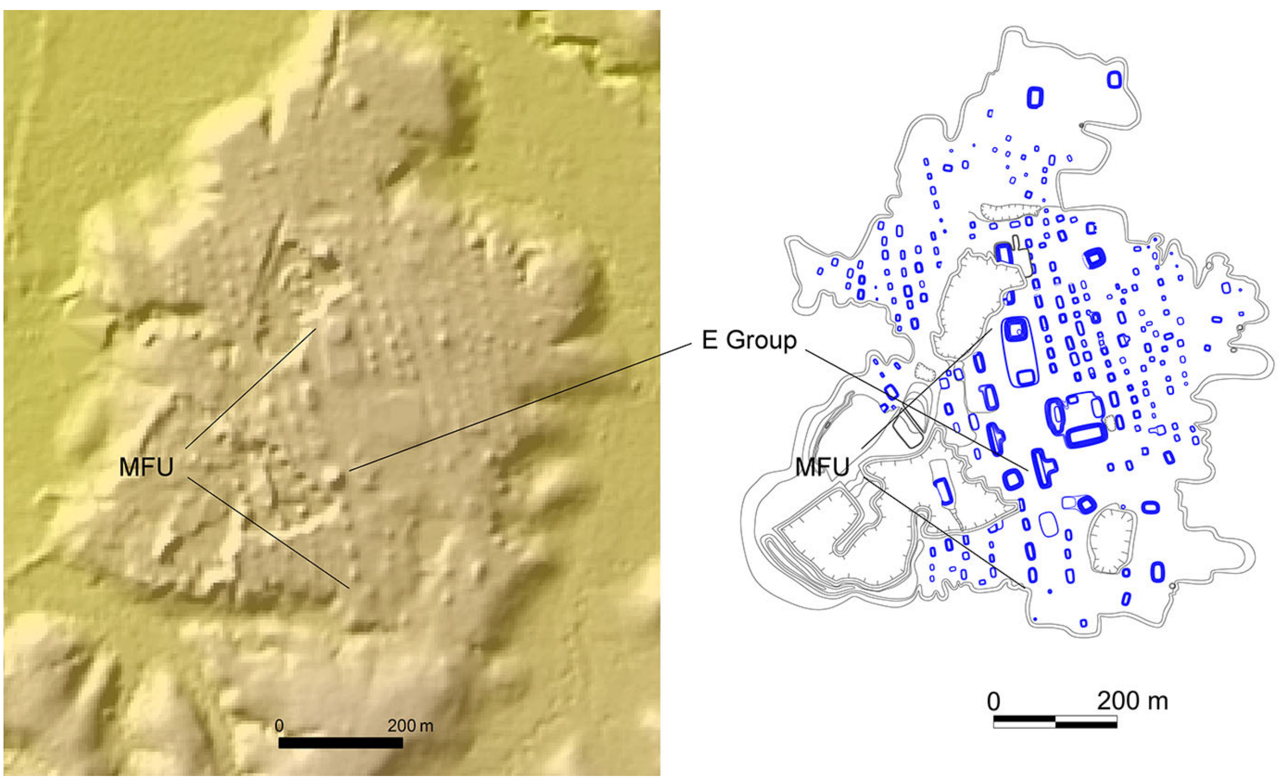

Supplementary Figure 5 │ Achotal-Gravera.

The MFU is somewhat obscured in the lidar-derived hillshade, but it is clearly recorded in the INAH map. The site was originally classified as a major centre during the lidar analysis, but after the comparison with the INAH data, it was classified also as an MFU.

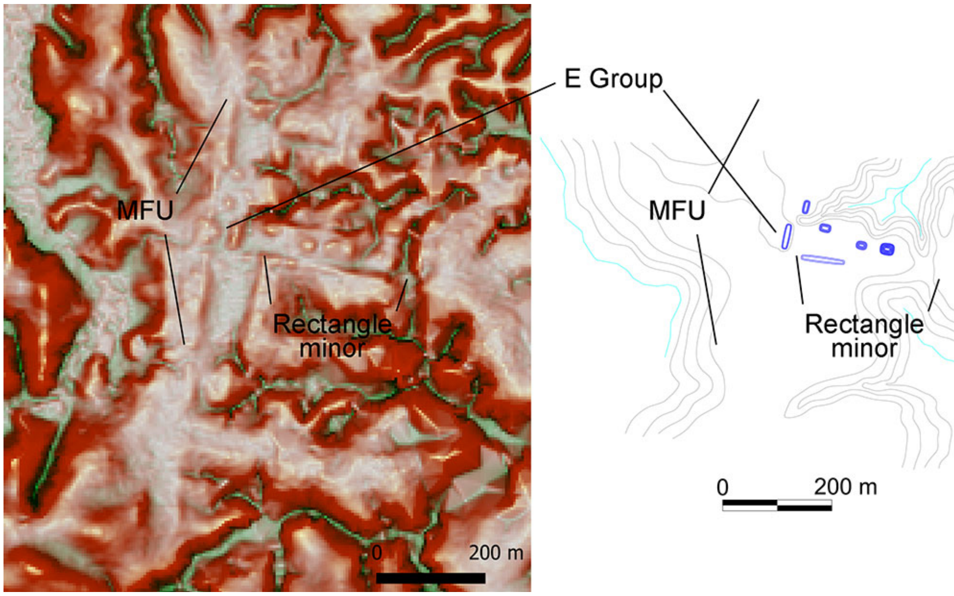

Supplementary Figure 6 │ Viva La Revolución II.

The VC and the minor rectangle made of low mound are visible in the lidar-derived RRIM but were not fully recognized during the INAH survey.

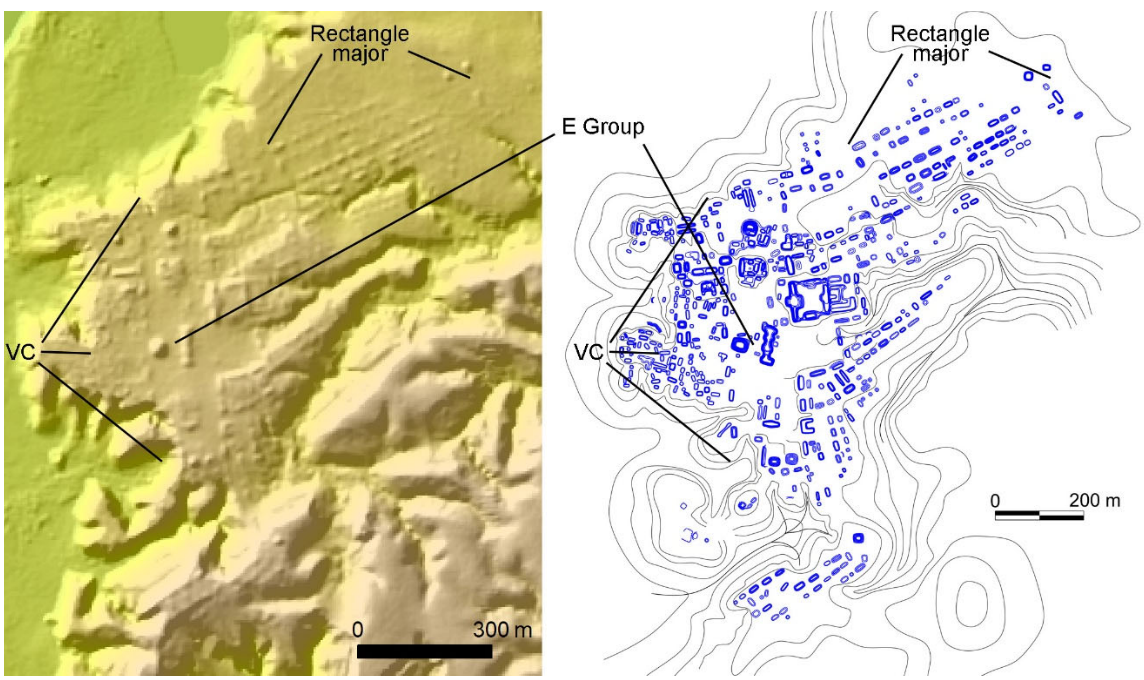

Supplementary Figure 7 │ Boca de Chalchijapan.

The VC is visible in the lidar-derived hillshade. It is also recorded in the INAH map, but somewhat unclearly. The major rectangle is visible in both images.

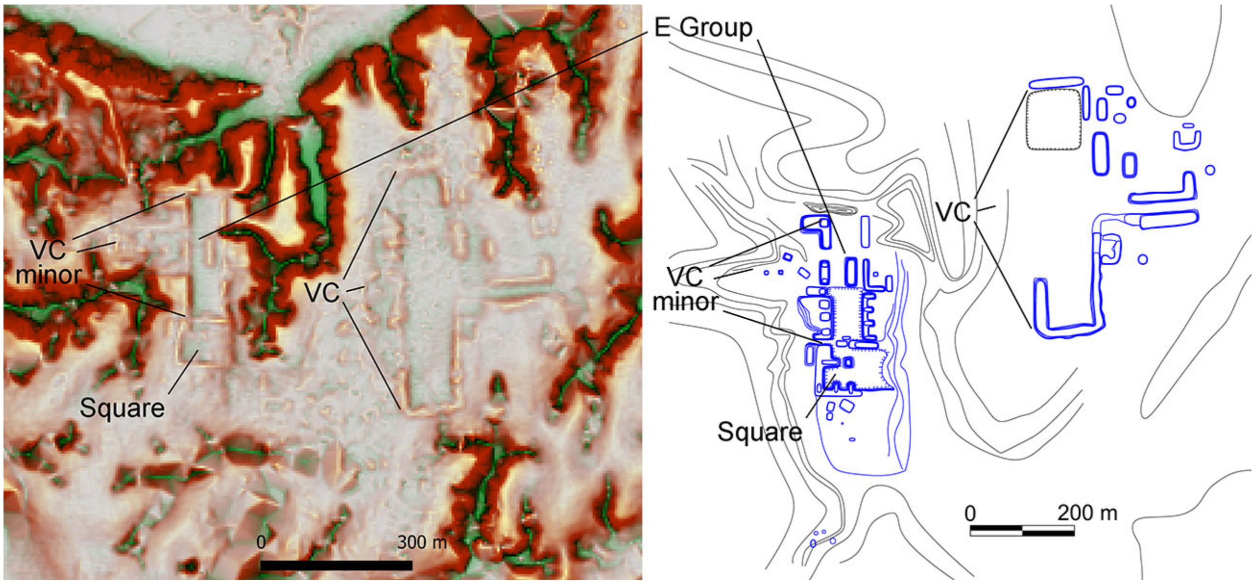

Supplementary Figure 8 | Río Abundancia.
The rectangle portion of the minor VC are visible both in the lidar-derived RRIM and in the INAH map, but its west wing was not fully recorded in the latter. The VC is visible in both images, but its western portion was not fully recognized during the INAH survey.

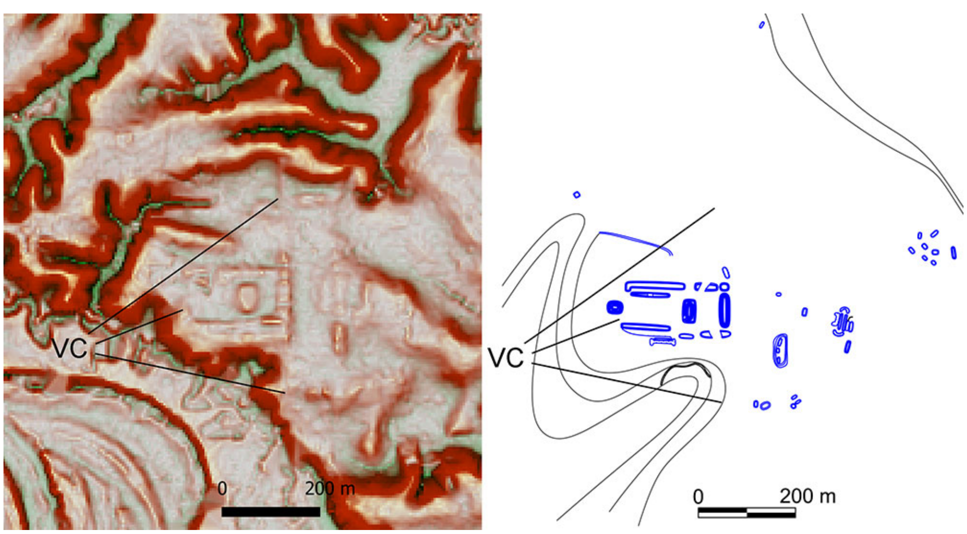

Supplementary Figure 9 | San Miguel.
The west wing of the VC is visible both in the lidar-derived RRIM and in the INAH, but its rectangular portion made of low mounds was not fully recognized during the INAH survey.

Supplementary Discussion 3: Subsistence and mobility

In the Gulf Olmec region, the use of ceramics and a certain level of sedentism were present around 1,800 BC, but there was probably variation in the degree of sedentism[1-5]. In the Middle Usumacinta region, the earliest confirmed ceramics date to around 1,200 BC[6-8]. A critical issue is the nature and scale of maize cultivation. In our study area, research at San Andrés near La Venta has shown that domesticated maize was present by 5,000 BC[9]. Whereas early studies assumed the importance of maize in Early Formative societies[5], an increasing number of scholars argue that maize made up a small portion of subsistence until 1,000 BC or so[1-3,10-17]. At the same time, preserved maize remains from the Gigante Cave, Honduras, indicate that maize cobs had reached substantial sizes by 2,000 BC, and the isotope analysis of human remains from rock shelters in southern Belize suggests that an increase in maize consumption occurred between 2,700 and 2,000 BC[18,19]. This question needs to be further examined in future research, but there was probably a significant variation in diet, subsistence and mobility within Mesoamerica and the study area during the Early Formative and early Middle Formative periods[16,20,21].

In the Middle Usumacinta region, the analysis of starch grains on grinding stones by Clarissa Cagnato suggests that maize was an important part of the diet during the Middle Formative period[6]. The stable isotope data on the individual buried in NR1 dating to 1,005-845 BC are consistent with this interpretation (AA-114513: $\delta^{13}C$ -11.3 ‰, $\delta^{15}N$ 11.3). At the same time, the analysis of faunal remains suggests that aquatic resources were a significant part of the diet during the late part of the Early Formative and the early part of the Middle Formative (1,250-750 BC) (Supplementary Table 6). The ratio of aquatic species in faunal remains declines afterwards. The reliance on maize probably increased from the Middle Formative to Late and Terminal Formative and to the Classic period, as is well documented at various sites in the Maya lowlands[22-25]. The builders of some MFUs, VCs and rectangular complexes during the early Middle Formative period may have retained certain levels of residential mobility. Terrains around various MFUs and VCs do not show traces of residential platforms or other land modifications (Extended Data Figs. 4, 5). This pattern contrasts with those of later sites, where residential platforms and associated land modifications are visible in lidar. The builders of MFUs and VCs may have lived in ephemeral structures and changed their residences periodically because of their heavy reliance on aquatic species and other wild resources or because of the cycle of swidden agriculture. This lifestyle is also implied by the scarcity of artefacts in the early layers at Buenavista and Rancho Zaragoza. At Aguada Fénix, however, our excavations recovered substantial quantities of artefacts. It is not clear whether Aguada Fénix had a larger sedentary population around it or whether these artefacts were deposited by a large number of mobile groups that gathered seasonally there for construction events and rituals.

Supplementary Table 6 | Faunal remains from Aguada Fénix.

Vertebrate bones were quantified by the number of specimens, and invertebrates were quantified by the minimum number of individuals. Note that the percentages of aquatic species are high before 700 BC, and they become lower during later periods.

		Late pat of the Early Formative 1250-1000 BC		Early part of the Middle Formative 1000-700 BC		Late part of the Middle Formative 700-350 BC		Late Formative 350-75 BC		Terminal Formative 75 BC-AD 250		Classic Period AD 250-950		Unknown/Mixe d Context		Total	
Scientific Name	Common Name	Freq.	%	Freq.	%	Freq.	%	Freq.	%	Freq.	%	Freq.	%	Freq.	%	Freq.	%
Terrestrial species																	
Didelphidae	opossums									1	0.5					1	0.1
Dasyprocta punctata	agouti											1	5.0			1	0.1
Mammalia, small	rodents, small carnivores			11	1.5			1	2.0	2	1.1			1	0.3	15	1.0
Canis lupus familiaris	domestic dogs			24	3.2			2	4.0	5	2.7					31	2.0
Tayassuidae	peccaries			2	0.3					5	2.7					7	0.5
Cervidae	deer			5	0.7			1	2.0	4	2.2			1	0.3	11	0.7
Mammalia, medium-large	large carnivores, artiodactyls			13	1.8	3	18.8	5	10.0	6	3.2	2	10.0			29	1.9
Mammalia, unknown	unidentified mammals			27	3.7	3	18.8	3	6.0	39	21.1	2	10.0	2	0.6	76	5.0
Aves	birds									2	1.1					2	0.1
Subtotal				**82**	**11.1**	**6**	**37.5**	**12**	**24.0**	**64**	**34.6**	**5**	**25.0**	**4**	**1.1**	**173**	**11.3**
Aquatic species																	
Testudines, freshwater	sliders, mud turtles			551	74.6	4	25.0	18	36.0	23	12.4	4	20.0	1	0.3	601	39.2
Anura	frogs, toads			1	0.1											1	0.1
Ariidae	catfish			1	0.1											1	0.1
Centropomus sp.	snook			1	0.1											1	0.1
Actinopterygii	unidentified fish			15	2.0			1	2.0							16	1.0
Crassostrea cf. *rhizophorae*	mangrove oysters							1	2.0	8	4.3	3	15.0	2	0.6	14	0.9
Unionidae	freshwater mussels	85	50.0	21	2.8	1	6.3	4	8.0	6	3.2	1	5.0	1	0.3	119	7.8
Pomacea flagellata	apple snails	85	50.0	67	9.1	5	31.3	14	28.0	84	45.4	7	35.0	347	97.7	609	39.7
Subtotal		**170**	**100.0**	**657**	**88.9**	**10**	**62.5**	**38**	**76.0**	**121**	**65.4**	**15**	**75.0**	**351**	**98.9**	**1362**	**88.7**
Total		**170**	**100.0**	**739**	**100.0**	**16**	**100.0**	**50**	**100.0**	**185**	**100.0**	**20**	**100.0**	**355**	**100.0**	**1535**	**100.0**

Supplementary Table 7 | Elevations of final San Lorenzo-phase floors (1,400-1,150/1,000 BC) reported by Michael Coe and Richard Diehl[5]

Edge Platform		Rectangular flat area		Difference
Edge Platform 2 (Mound C2-10)	74.6 m	Area in front	73.6 m	c. 1.0 m
Edge Platform 5	77.0-77.2 m	Central part	74.5-74.6 m	c. 2.5 m
Around Monument 51 south of the Villa Alta complex			73.7 m	

Supplementary Discussion 4: Radiocarbon dating

We established a basic chronology of the Middle Usumacinta region in our previous study with 69 radiocarbon dates[6]. Here we present 33 additional radiocarbon dates that we obtained in 2020 (Extended Data Fig. 8, Supplementary Table 8). These new dates largely confirm our original chronology. Some sites in our study area (for example, La Venta, San Lorenzo, Tres Zapotes, El Marquesillo, Matacapan, Comalcalco, Moral-Reforma, Pomona, Palenque, Chinikiha, El Tigre, and Aguacatal) were investigated by other scholars[26-35]. Likewise, our discussion mentions the dates of sites located outside our study area (for example, Chiapa de Corzo, San Isidro, La Libertad, Ojo de Agua, La Blanca, and Ceibal) based on earlier studies conducted by various scholars[36-45].

The new samples were obtained from Ops. NR5B, AF1D, BV1A and ZR1A of the 2020 field season and from Ops. NR7A, NR8A, AF2B and TR1A of previous seasons. They were analyzed at the University of Arizona Accelerated Mass Spectrometry (AMS) lab. We conducted the Bayesian analysis of the radiocarbon dates using Oxcal 4.4.3 software (https://c14.arch.ox.ac.uk/oxcal/OxCal.html) and IntCal20 calibration data[46,47] (Supplementary Method). The method and procedure of Bayesian analysis have been discussed previously in detail[6,44,48-52]. An important issue is the identification of problematic radiocarbon dates (outliers). To address this problem, scholars have used two methods: (1) the manual or subjective rejection of outliers; and (2) outlier models, which automatically identify outliers and correct modelled dates through statistical modelling[53,54]. In this study, we used both methods with a stronger emphasis on the first (manual rejection), which allows us to evaluate individual radiocarbon dates considering their specific contexts and comparing them with existing ceramic chronologies. The graphic presentation of the results shown in Extended Data Fig. 8 and the modelled dates listed in Supplementary Table 8 are based on the manual rejection models. The agreement indices and convergence values in Supplementary Table 8 also resulted from the manual rejection models, whereas the posterior outlier probabilities derived from the outlier models. The outlier model of the 2019 data was published in our previous publication[6].

In analyzing this dataset, we need to consider the possible presence of radiocarbon dates older than their deposition dates (samples with inbuilt age) because of old wood and redeposited charcoal pieces. In Mesoamerica, structures are often constructed over existing buildings, and materials from earlier fills and deposits are commonly incorporated in the fills of the new buildings. Moreover, in lowland Mesoamerica, including our field research area, the preservation of organic materials is poor, and seeds and other short-lived plant remains are scarce. This problem is particularly serious for the 2020 collection because it consisted mostly of samples obtained from construction fills, in contrast to the 2019 dataset, which included a reasonable number of samples from middens and other better contexts. In the manual rejection model, we often rejected the samples that were older than the dates of associated ceramics or other samples from the same or upper layers. In addition, AA-114531 was probably a modern root and was excluded. In the outlier models for the 2020 collection, we used the "Charcoal" outlier model for most samples with carbon contexts greater than 40 %. The "Charcoal" outlier model assumes that the samples may have inbuilt age. For AA-114524 with carbon content greater than 40 %, however, we used the "General" outlier model, which assumes that the radiocarbon date may be older or younger than the deposition date[53-55]. We also used the "General" outlier model for the bone samples from burials (AA-114511 and AA-114512).

Another issue is that ten of the 2020 samples had carbon content less than 40 %, which suggests that they were mixed with soils. In the tropical environment of the study area, many charcoal samples are poorly preserved. They easily fall apart and become powdery fragments. This problem is exacerbated for samples from construction fills. Powdery charcoal may be mixed with the surrounding soils during sample preparation. The effects of mixed soils depend on the quantity of the included soils, the carbon content of the soils, and the age of the insoluble soil carbon (humins) that remain after the acid-base-acid (ABA) pretreatment. Three samples with low carbon content (AA-114520, AA-114528 and AA-114532) have clearly anomalous dates and were not included in the models. In the outlier model, we applied the "General" outlier model to other samples with low carbon content. Although we suspect that humins tend to be older than the deposition date, the inclusion of younger soil carbon may also be possible. After the analysis, we tentatively accepted four samples with low carbon content (AA-114514, AA-114516, AA-114517 and AA-114537). However, these samples need to be further examined in future studies.

Our previous excavation in the southern part of the Main Plateau of Aguada Fénix (Op. NR3A) provided six radiocarbon dates from the deepest layer found directly on bedrock, which contained numerous ceramic sherds and faunal remains. These dates concentrated around 1,200 BC, but it was not clear whether this layer represented the earliest construction fill of the plateau or whether it was a midden deposited prior to the construction of the plateau. The analysis of faunal remains from this deposit identified 140 valves of freshwater clams, *Utterbackia imbecillis* (Supplementary Table 6). Many valves were stacked one on another with little soil in between, and the external membranes of some shells were preserved. Because these membranes begin to peel off quickly when they become dry, their good preservation and the stacking of shells suggest that this deposit is more likely a midden placed originally in this location rather than a fill with materials taken from different locations. This observation favours the interpretation that the dates around 1,200 BC (modelled start date 1,300-1,130 BC, 95.4 % range) represent human activities predating the plateau construction. A human bone from Burial NR1 of Op. NR7A had a low collagen yield, but the resulting date (AA-114513, calibrated date 1,010-835 BC, modelled date 970-845 BC) is consistent with other valid dates from this operation. This date supports the previous interpretation that the construction of the Main Plateau started by 1,050 or 1,000 BC (modelled start date 1,140-980 BC). Nonetheless, as we did not find any carbon sample from the initial plateau construction layers from Op. NR3A, in future studies we still need to explore the possibility that the plateau construction started earlier.

The new dates from Floors 9 and 10 in Op. NR5B (AA-114529 and AA-114537) placed in the Aguada Fénix E-Group plaza fall around 900 BC and are consistent with the chronology of plateau constructions. We had to close this excavation before we reach bedrock because of the spread of COVID-19. AA-114530 from Floor 6 of this excavation has a wide range between 780 and 545 BC because of the flat area of the calibration curve during this period, but the highest probability is found around 760 and 750 BC. If this date is valid, the construction of the plateau may have continued until around 750 BC. For the MFU site of La Carmelita, the 2019 model suggested an end data of 770-430 BC with the highest probability around 740 BC. Activity at both Aguada Fénix and La Carmelita may have ceased around 750 or 740 BC. Ceramic data suggest that a small population returned to Aguada Fénix during the Terminal Formative period. AA-114508 from Op. NR8A (45 BC-AD 125) confirms this interpretation.

In Op. AF1D placed in an Aguada Fénix peripheral area, six samples were taken from the deposits made of soils of multiple colours. This deposit included fragments of human bones, which appear to have been taken from burials located in a different location and included in the fill. Aguada Fénix Stone Sculpture 1, or "Choco," was also found in this deposit. Many artefacts and carbon pieces in this deposit appear to have been transposed from different locations, and thus some dates are probably earlier than the deposition at this location. We interpret AA-114516 and AA-114517 as valid dates. AA-114519 may be somewhat earlier than the deposition date but is in an acceptable range. The Bayesian model suggests a date range of 1,055-605 BC with the highest probability around 830-770 BC for this deposit. A date from a later intrusion (AA-114514) is consistent with this interpretation.

The quantity of artefacts recovered from the MFU site of Buenavista was small, and we did not find any ceramics in the fill of Floor 5 in Op. BV1A, which appears to represent the initial construction of the E-Group eastern platform. We found many pieces of charcoal in the fill of Floor 5 and dated six of them. Most samples returned significantly old dates, suggesting that they are old charcoal included in soils taken for the fills. Only AA-114524 yielded a date (calibrated date 775 and 425 BC with the highest probability around 760 and 740 BC) consistent with the final Middle Formative construction stages at Aguada Fenix and La Carmelita. The chronology of this site needs to be further examined with more data.

We also found only a small quantity of artefacts in lower layers of Op. ZR1A at the MFC site of Rancho Zaragoza. The fill of Floor 8 represents the initial construction of this MFC complex. A small number of sherds from this context appears to include Joventud Red of the late Middle Formative Mamom phase (700-350 BC). AA-114539 found directly on Floor 8 provided a calibrated date of 750-405 BC, which is consistent with this ceramic dating. Ceramic data suggest that the occupation of this site continued through the Late and Terminal Formative periods. Ceramic data from the MFC site of El Tiradero indicate that this site was constructed mostly during the Late and Terminal Formative periods. AA-114505 from Op. TR1A returned a calibrated date range of 375-195 BC. We list this as an acceptable date, but it may be somewhat older than its deposition date. The site was reoccupied toward the end of the Late Classic period. AA-114511 and AA-114512 from Burials TR1 and TR2 gave dates of AD 670-820 and AD 675-825, respectively.

In sum, most MFU sites in the Middle Usumacinta region were probably constructed between 1,050 and 750 BC, although we still need to examine the possibility that the construction of the Main Plateau at Aguada Fénix started earlier. After the probable abandonment around 750 BC, some MFU complexes were reoccupied in the late part of the Late Formative period or during the Terminal Formative period. By then, the original meaning of the standardized complexes may have been lost. We suspect that most of the MFC and MFG complexes found in central and western Tabasco and northwestern Chiapas of our study area date to the heyday of La Venta and the MFC centres in the Chiapas Grijalva River region between 800 and 400 BC. However, the MFC sites in the Middle Usumacinta region may have started later and continued after the decline of La Venta and some Chiapas MFC centres around 400 BC. In particular, the Late and Terminal Formative dates of El Tiradero are unique among MFC centres, and its implications need to be examined in future research.

Supplementary Method: Oxcal code

1. Oxcal code for the modified 2019 Bayesian model: Manual rejection of outliers

AA-114507, AA-114508 and AA-114513 obtained in 2020 were added to the 2019 model published in [6]. See Supplementary Table 8 for the results.

```
Plot()
 {
  Sequence("Aguada Fénix Op NR3A")
  {
   Label("Aguada Fénix midden before plateau construction (Op NR3A)");
   Boundary("Start midden NR3A");
   Phase("Midden")
   {
    R_Date("TKA-20626 NR3A4-8-9 midden", 2989, 25);
    R_Date("TKA-20627 NR3A4-8-9 midden", 2951, 24);
    R_Date("TKA-20628 NR3A4-8-10 midden", 2987, 26);
    R_Date("TKA-20629 NR3A4-8-10 midden", 3016, 24);
    R_Date("TKA-20630 NR3A4-8-10 midden", 2977, 28);
    R_Date("TKA-20631 NR3A4-8-10 midden", 2949, 23);
   };
   Boundary("End midden NR3A");
   Label("Aguada Fénix Main Plateau (Op NR3A)");
   Boundary("Start Main Plateau NR3A");
   Phase("Colour fill")
   {
    R_Date("TKA-20622 NR3A3-7-3 colour fill", 2832, 23);
    R_Date("TKA-20623 NR3A2-7-1 colour fill", 2848, 24);
    R_Date("TKA-20624 NR3A2-7-1 colour fill", 2869, 24);
    R_Date("TKA-20625 NR3A2-7-4 colour fill", 2848, 23);
   };
   Boundary("NR3A Floor 10");
   Boundary("NR3A Floor 7b");
   R_Date("TKA-20621 NR3A4-6-3 Under Floor 6", 2743, 23);
   Boundary("NR3A Floor 6");
   R_Date("TKA-20620 NR3A4-6-2 Under Floor 5", 2701, 26);
   Boundary("End Middle Formative NR3A");
  };
  Sequence("Aguada Fénix Op NR7A")
  {
   Label("Aguada Fénix midden before plateau construction (Op NR7A)");
   Boundary("Start midden NR7A");
   R_Combine("TKA-21342&TKA-21343 NR7A3-8-6")
   {
    R_Date("TKA-21342 NR7A3-8-6* Cache NR2", 2941, 21);
    R_Date("TKA-21343 NR7A3-8-6* Cache NR2", 2940, 19);
   };
   Boundary("NR7A Cache-fill");
   Phase("Floor 11 fill")
   {
    R_Date("TKA-21341 NR7A3-8-4 Fill on bedrock", 2929, 21);
    R_Date("TKA-21345 NR7A1-8-4 Floor 11 fill", 2867, 19);
   };
```

```
  Boundary("End midden NR7A");
  Label("Aguada Fénix Main Plateau (Op NR7A)");
  Boundary("Start Main Plateua NR7A");
  R_Date("TKA-21340 NR7A3-8-1 Floor 10 fill",
2817, 19);
  Boundary("NR7A Floor 10");
  R_Date("TKA-21344 NR7A2-7-3x Fill", 2994, 20)
  {
   Outlier();
  };
  R_Date("TKA-21339 NR7A1-7-1x Floor 8 fill",
3230, 20)
  {
   Outlier();
  };
  Boundary("NR7A Floor 6");
  R_Date("AA-114513 NR7A3-5-4 Burial NR1",
2783, 28);
  Boundary("NR7A Floor 5");
  Phase("NR7A ceramic offering")
  {
   R_Date("TKA-21337 NR7A3-4-4x Ceramic
offering", 3136, 21)
   {
    Outlier();
   };
   R_Date("TKA-21338 NR7A3-4-4 Ceramic
offering", 2718, 19);
  };
  Boundary("End Middle Formative NR7A");
  Phase("Terminal Formative")
  {
   R_Date("TKA-21336 NR7A1-4-2x Floor 2 fill",
4992, 22)
   {
    Outlier();
   };
   R_Date("TKA-21335 NR7A2-4-2 Floor 2 fill",
2889, 19)
   {
    Outlier();
   };
  };
  Boundary("End Terminal Formative NR7A");
 };
 Sequence("Aguada Fénix Op NR5A")
 {
  Boundary("Start NR5A");
  R_Date("TKA-20670 NR5A2-7-8 Floor 23 fill",
3017, 23);
  Boundary("NR5A Floor 23");
  Label("Aguada Fénix Main Plateau (Op NR5A)");
  Boundary("Start Main Plateau NR5A");
  Sequence("NR5A Main Plateau Middle
Formative")
  {
   Boundary("Start NR5A Floor 22 fill");
   Phase("Floor 22 fill")
   {
    R_Date("TKA-20668 NR5A1-7-5 Under Floor
22", 2805, 21);
    R_Date("TKA-20669 NR5A1-7-8 Floor 22 fill",
2834, 20);
   };
   Boundary("NR5A Floor 22");
   R_Date("TKA-20638 NR5A1-6-13 Floor 19 fill",
3800, 25)
   {
    Outlier();
   };
   Boundary("NR5A Floor 19");
   R_Date("TKA-20637 NR5A1-6-6 On Floor 16",
2845, 23);
   Boundary("NR5A Floor 15");
   R_Date("TKA-20635 NR5A2-6-4 On Floor 14",
2835, 25);
   Boundary("NR5A Floor 13");
```

```
   R_Date("TKA-20636 NR5A2-6-3 On Floor 13", 2838, 23);
   Boundary("NR5A Floor 12");
  };
  Boundary("End Middle Formative NR5A");
  Boundary("Start Late-Terminal Formative NR5A");
  R_Date("TKA-20634 NR5A2-4-4 On Floor 4", 2055, 22);
  Boundary("End Late-Terminal Formative NR5A");
 };
 Sequence("Aguada Fénix Op NR8A")
 {
  Label("Aguada Fénix Main Plateau (Op NR8A)");
  Boundary("Start Main Plateau NR8A");
  Sequence("NR8A Main Plateau Middle Formative")
  {
   Boundary("NR8A Floor 19");
   Phase("NR8A on Floor 19")
   {
    R_Date("TKA-21370 NR8A8-6-9 On Floor 19", 2874, 22);
    R_Date("TKA-21371 NR8A8-6-9 On Floor 19", 2879, 22);
   };
   Boundary("NR8A Floor 18");
   Boundary("NR8A Floor 14");
   Phase("NR8A Floor 13 fill")
   {
    R_Date("TKA-21368 NR8A1-5-3 Floor 13 fill", 2800, 22);
    R_Date("TKA-21369 NR8A2-5-3 Floor 13 fill", 2781, 25);
   };
   Boundary("NR8A Floor 13");
   Boundary("NR8A Floor 5");
   R_Date("TKA-21367 NR8A1-4-4 Floor 4 fill", 2772, 24);
   Boundary("NR8A Floor 4");
   R_Date("TKA-21366 NR8A1-4-3 On Floor 4", 2728, 24);
   Boundary("NR8A Floor 3");
  };
  Boundary("End Middle Formative NR8A");
  Boundary("Start Terminal Formative NR8A");
  R_Date("AA-114508 NR8A7-4-2 On Floor 3", 1976, 34);
  Boundary("End Terminal Formative NR8A");
  Boundary("Start Late Classic NR8A");
  R_Date("TKA-21365 NR8A5-3-1 Termination deposit", 1242, 25);
  Boundary("End Late Classic NR8A");
 };
 Sequence("Aguada Fénix causeway Op NR4A")
 {
  Label("Aguada Fénix causeway (Op NR4A)");
  Boundary("Start causeway NR4A");
  R_Date("TKA-20633 NR4A1-7-6 Floor 18 fill", 2785, 23);
  Boundary("NR4A Floor 18");
  Boundary("NR4A Floor 10");
  R_Date("TKA-20632 NR4A1-5-6 On Floor 10", 2753, 23);
  Boundary("End causeway NR4A");
 };
 Sequence("Aguada Fénix causeway Op NR6A")
 {
  Label("Aguada Fénix causeway (Op NR6A)");
  Boundary("Start causeway NR6A");
  R_Date("TKA-20680 NR6A1-6-6 Floor 23 fill", 2726, 20);
  Boundary("NR6A Floor 23");
  Boundary("NR6A Floor 22");
  Phase("Floor 21 fill")
  {
   R_Date("TKA-20679 NR6A1-6-3 Floor 21 fill", 2759, 20)
   {
```

```
   Outlier();
  };
  R_Date("TKA-20678 NR6A1-6-3 Floor 21 fill", 2689, 21);
  R_Date("TKA-20677 NR6A1-6-2 Floor 21 fill", 2927, 20)
  {
   Outlier();
  };
 };
 Boundary("NR6A Floor 21");
 Boundary("NR6A Floor 20");
 R_Date("TKA-20676 NR6A1-5-26 Canal 5", 2677, 20);
 Boundary("NR6A Floor 19");
 Boundary("NR6A Floor 17");
 Phase("Floor 16 & Canal 3")
 {
  R_Date("TKA-20672 NR6A1-5-18 Floor 16 fill", 2778, 20)
  {
   Outlier();
  };
  R_Date("TKA-20673 NR6A1-5-18 Floor 16 fill", 2730, 20);
  R_Date("TKA-20675 NR6A1-5-19 In Canal 3", 2756, 20)
  {
   Outlier();
  };
  R_Date("TKA-20674 NR6A1-5-19 In Canal 3", 2718, 20);
 };
 Boundary("NR6A Floor 15");
 R_Date("TKA-20671 NR6A1-5-15 Canal 2", 2756, 20)
 {
  Outlier();
 };
 Boundary("End causeway NR6A");
 };
 Sequence("Aguada Fénix peripheral area Op AF1A")
 {
 Boundary("Start AF1A");
 Phase("AF1A Carbon layer")
  {
  R_Date("TKA-21323 AF1A1-5-1 carbon layer", 2742, 19);
  R_Date("TKA-21324 AF1A1-5-1 carbon layer", 2717, 19);
  };
 Boundary("AF1A Floor 2");
 };
 Sequence("Aguada Fénix peripheral area Op AF1B")
 {
 Boundary("Start AF1B");
 R_Date("TKA-21327 AF1B1-6-6 In Floor 14", 2847, 19);
 Boundary("AF1B Floor 14");
 Boundary("AF1B Floor 9");
 R_Date("TKA-21326 AF1B1-5-5 Floor 8 fill", 2809, 19);
 Boundary("AF1B Floor 8");
 Boundary("AF1B Floor 6");
 R_Date("TKA-21325 AF1B1-5-1 Floor 4 fill and part of Floor 5", 2742, 20);
 Boundary("AF1B Floor 4");
 };
 Sequence("Aguada Fénix peripheral area Op AF2B")
 {
 Boundary("Start AF2B");
 Phase("AF2B midden")
  {
  R_Date("TKA-21330 AF2B1-5-3x Floor 10 fill", 3340, 21)
   {
```

```
    Outlier();
   };
   R_Date("TKA-21329 AF2B1-5-3 Floor 10 fill", 2678, 19);
  };
  Boundary("AF2B Floor 10");
  Boundary("AF2B Floor 5");
  Phase("AF2B Floor 4 fill")
  {
   R_Date("AA-114507 AF2B1-4-6 Floor 4 fill", 2564, 30);
   R_Date("TKA-21328 AF2B1-4-6 Floor 4 Fill", 2519, 19);
  };
  Boundary("AF2B Floor 4");
 };
 Sequence("La Carmelita Op LC1B")
 {
  Boundary("Start La Carmelita LC1B");
  Phase("LC1B lower fill")
  {
   R_Date("TKA-20613 LC1B1-5-6", 2772, 23);
   R_Date("TKA-20614 LC1B1-5-6", 2746, 23);
   R_Date("TKA-20615 LC1B1-5-7", 2750, 23);
   R_Date("TKA-20616 LC1B1-5-8", 2782, 26);
   R_Date("TKA-20617 LC1B1-5-8", 2751, 24);
   R_Date("TKA-20618 LC1B1-5-8", 2775, 23);
   R_Date("TKA-20619 LC1B1-5-10", 2469, 25)
   {
    Outlier();
   };
  };
  Boundary("End La Carmelita LC1B");
 };
 Sequence("La Carmelita Op LC3A")
 {
  Boundary("Start La Carmelita LC3A");
  Phase("LC3A Floor 2d fill")
  {
   R_Date("TKA-21334 LC3A1-5-11x Floor 2d fill", 3723, 21)
   {
    Outlier();
   };
   R_Date("TKA-21333 LC3A1-5-11  Floor 2d fill", 2733, 20);
  };
  Boundary("LC3A Floor 2d");
  Boundary("LC3A Floor 2c");
  Phase()
  {
   R_Date("TKA-21331 LC3A1-5-2 Floor 2c fill", 2481, 19);
   R_Date("TKA-21332 LC3A1-5-2 Floor 2c fill", 2508, 20);
  };
  Boundary("End La Carmelita LC3A");
 };
};
```

2. Oxcal code for the 2020 Bayesian model: Manual rejection of outliers

AA-114507, AA-114508 and AA-114513 obtained in 2020 were added to the modified 2019 model. See Extended Data Fig. 8 and Supplementary Table 8 for the results.

```
Plot()
 {
  Sequence("AF1D")
  {
   Boundary("Start colored fill");
   Phase("Color fill")
   {
    R_Date("AA-114521 AF1D1-5-8 Burial AF1",
3352, 41)
    {
     Outlier();
    };
    R_Date("AA-114519 AF1D1-5-8 Burial AF1",
2721, 26);
    R_Date("AA-114518 AF1D1-5-7 Cache AF1",
2979, 26)
    {
     Outlier();
    };
    R_Date("AA-114516 AF1D1-5-7 Cache AF1",
2579, 28);
    R_Date("AA-114517 AF1D1-5-7 Cache AF1",
2536, 84);
    R_Date("AA-114520 AF1D1-5-8 Burial AF1",
909, 88)
    {
     Outlier();
    };
   };
   Boundary("Color fill-instrusion");
   Phase("intrusion")
   {
    R_Date("AA-114515 AF1D1-5-2 Intrusion", 2969,
28)
    {
     Outlier();
    };
    R_Date("AA-114514 AF1D1-5-2 Intrusion", 2514,
26);
   };
   Boundary("End intrusion");
  };
  Sequence("NR5B")
  {
   Boundary("Floor 10");
   R_Date("AA-114537 NR5B3-5-4 On Floor 10",
2748, 52);
   Boundary("Floor 9");
   R_Date("AA-114529 NR5B1-5-2 On Floor 9",
2768, 26);
   Boundary("Floor 8");
   Phase("On Floor 8")
   {
    R_Date("AA-114528 NR5B2-5-1 On Floor 8",
11221, 38)
    {
     Outlier();
    };
    R_Date("AA-114533 NR5B3-5-1 On Floor 8",
2882, 28)
    {
     Outlier();
    };
    R_Date("AA-114534 NR5B3-5-1 On Floor 8",
2875, 26)
    {
     Outlier();
```

```
   };
  };
  Boundary("Floor 7");
  Phase("Caches")
  {
   R_Date("AA-114532 NR5B2-5-5 Cache NR3", 12100, 39)
   {
    Outlier();
   };
   R_Date("AA-114536 NR5B2-5-6 Cache NR4", 2884, 29)
   {
    Outlier();
   };
  };
  Boundary("Floor 6");
  R_Date("AA-114530 NR5B4-4-8 On Floor 6", 2499, 25);
  Boundary("Floor 5");
 };
 Sequence("BV1A")
 {
  Boundary("Start Floor 5 fill");
  Phase("BA1A lower fill")
  {
   R_Date("AA-114522 BV1A1-5-1 Floor 5 fill", 4485, 27)
   {
    Outlier();
   };
   R_Date("AA-114527 BV1A1-5-4 Floor 5 fill", 3881, 27)
   {
    Outlier();
   };
   R_Date("AA-114525 BV1A1-5-1 Floor 5 fill", 3753, 27)
   {
    Outlier();
   };
   R_Date("AA-114523 BV1A1-5-1 Floor 5 fill", 3328, 26)
   {
    Outlier();
   };
   R_Date("AA-114526 BV1A1-5-1 Floor 5 fill", 2989, 35)
   {
    Outlier();
   };
   R_Date("AA-114524 BV1A1-5-1 Floor 5 fill", 2481, 33);
  };
  Boundary("End Floor 5 fill");
 };
 Sequence("ZR1A")
 {
  Boundary("Start");
  R_Date("AA-114540 ZR1A1-5-2 Floor 8 fill", 3120, 26)
  {
   Outlier();
  };
  Boundary("ZR Floor 8");
  R_Date("AA-114539 ZR1A1-5-1 On Floor 8", 2430, 26);
  Boundary("ZR Floor 7");
  R_Date("AA-114538 ZR1A1-4-6 On Floor 5", 2891, 26)
  {
   Outlier();
  };
  Boundary("ZR Floor 4");
 };
 Sequence("TR1A&2B")
 {
  Boundary("Start TR1A Terminal Preclassic");
```

```
 Phase("TR1A Floor 2 fill")
 {
  R_Date("AA-114504 TR1A1-5-1 Floor 2 fill",
2926, 24)
  {
   Outlier();
  };
  R_Date("AA-114505 TR1A1-5-2 Floor 2 fill",
2215, 20);
 };
 Boundary("TR1A End Terminal Preclassic");
 Boundary("TR2B Start Late Classic");
 Sequence("Late Classic")
 {
  Boundary("TR2B Floor 2");
  Phase("TR2B Burials")
  {
   R_Date("AA-114511 TR2B3-4-2 Burial TR1",
1266, 25);
   R_Date("AA-114512 TR2B2-4-3 Burial TR2",
1246, 29);
  };
  Boundary("TR2B Floor 1");
  };
  Boundary("TR2B End Late Classic");
 };

Date(Prior("AA_114513_NR7A3_5_4_Burial_NR1_
modelled2","AA_114513_NR7A3_5_4_Burial_NR1
_modelled2.prior"););

Date(Prior("AA_114513_NR7A3_5_4_Burial_NR1_
unmodelled2","AA_114513_NR7A3_5_4_Burial_N
R1_unmodelled2.prior"););

Date(Prior("AA_114507_AF2B1_4_6_Floor_4_fill_
modelled2","AA_114507_AF2B1_4_6_Floor_4_fill_
modelled2.prior"););

Date(Prior("AA_114507_AF2B1_4_6_Floor_4_fill_
unmodelled2","AA_114507_AF2B1_4_6_Floor_4_fi
ll_unmodelled2.prior"););

Date(Prior("AA_114508_NR8A7_4_2_On_Floor_3_
modelled2","AA_114508_NR8A7_4_2_On_Floor_3
_modelled2.prior"););

Date(Prior("AA_114508_NR8A7_4_2_On_Floor_3_
unmodelled2","AA_114508_NR8A7_4_2_On_Floor
_3_unmodelled2.prior"););
 };
```

3. Oxcal code for the 2020 Bayesian model: Outlier model

```
Plot()
 {
  Outlier_Model("General",T(5),U(0,4),"t");
  Outlier_Model("Charcoal",Exp(1,-10,0),U(0,3),"t");
  Sequence("AF1D")
  {
   Boundary("Start coloured fill");
   Phase("Coloured fill")
   {
    R_Date("AA-114518 AF1D1-5-7 Cache AF1",
2979, 26)
    {
     Outlier("Charcoal",1);
    };
    R_Date("AA-114519 AF1D1-5-8 Burial AF1",
2721, 26)
    {
     Outlier("General",0.05);
    };
   };
   Boundary("End Coloured fill");
  };
  Sequence("NR5B")
  {
   Boundary("Floor 9");
   R_Date("AA-114529 NR5B1-5-2 On Floor 9",
2768, 26)
   {
    Outlier("Charcoal",1);
   };
   Boundary("Floor 8");
   Phase("On Floor 8")
   {
    R_Date("AA-114533 NR5B3-5-1 On Floor 8",
2882, 28)
    {
     Outlier("Charcoal",1);
    };
    R_Date("AA-114534 NR5B3-5-1 On Floor 8",
2875, 26)
    {
     Outlier("Charcoal",1);
    };
   };
   Boundary("Floor 7");
   Phase("Caches")
   {
    R_Date("AA-114536 NR5B2-5-6 Cache NR4",
2884, 29)
    {
     Outlier("Charcoal",1);
    };
   };
   Boundary("Floor 6");
   R_Date("AA-114530 NR5B4-4-8 On Floor 6",
2499, 25)
   {
    Outlier("General",0.05);
   };
   Boundary("Floor 5");
  };
  Sequence("BV1A")
  {
   Boundary("Start Floor 5 fill");
   Phase("BA1A lower fill")
   {
    R_Date("AA-114522 BV1A1-5-1 Floor 5 fill",
4485, 27)
    {
     Outlier("Charcoal", 1);
    };
```

```
   R_Date("AA-114527 BV1A1-5-4 Floor 5 fill",
3881, 27)
   {
    Outlier("Charcoal", 1);
   };
   R_Date("AA-114525 BV1A1-5-1 Floor 5 fill",
3753, 27)
   {
    Outlier("Charcoal", 1);
   };
   R_Date("AA-114523 BV1A1-5-1 Floor 5 fill",
3328, 26)
   {
    Outlier("Charcoal", 1);
   };
   R_Date("AA-114526 BV1A1-5-1 Floor 5 fill",
2989, 35)
   {
    Outlier("Charcoal", 1);
   };
   R_Date("AA-114524 BV1A1-5-1 Floor 5 fill",
2481, 33)
   {
    Outlier("General", 0.05);
   };
  };
  Boundary("End Floor 5 fill");
 };
 Sequence("ZR1A")
 {
  Boundary("ZR Floor 8");
  R_Date("AA-114539 ZR1A1-5-1 On Floor 8",
2430, 26)
  {
   Outlier("Charcoal", 1);
  };
  Boundary("ZR Floor 7");
  R_Date("AA-114538 ZR1A1-4-6 On Floor 5",
2891, 26)
  {
   Outlier("Charcoal", 1);
  };
  Boundary("ZR Floor 4");
 };
 Sequence("TR1A&2B")
 {
  Boundary("Start TR1A Terminal Formative");
  Phase("TR1A Floor 2 fill")
  {
   R_Date("AA-114504 TR1A1-5-1 Floor 2 fill",
2926, 24)
   {
    Outlier("Charcoal",1);
   };
   R_Date("AA-114505 TR1A1-5-2 Floor 2 fill",
2215, 20)
   {
    Outlier("General",0.05);
   };
  };
  Boundary("TR1A End Terminal Formative");
  Boundary("TR2B Start Late Classic");
  Sequence("Late Classic")
  {
   Boundary("TR2B Floor 2");
   Phase("TR2B Burials")
   {
    R_Date("AA-114511 TR2B3-4-2 Burial TR1",
1266, 25)
    {
     Outlier("General",0.05);
    };
    R_Date("AA-114512 TR2B2-4-3 Burial TR2",
1246, 29)
    {
     Outlier("General",0.05);
    };
```

```
 };
 Boundary("TR2B Floor 1");
};
```

```
 Boundary("TR2B End Late Classic");
 };
};
```

References

1 Arnold, P. J., III. Settlement and subsistence among the Early Formative Gulf Olmec. *Journal of Anthropological Archaeology* **28**, 397-411 (2009).

2 Arnold, P. J., III. in *Olmec art and archaeology in Mesoamerica* (eds John E. Clark & Mary E. Pye) 117-135 (National Gallery of Art, 2000).

3 Arnold, P. J., III. in *Pottery and people: a dynamic interaction* (eds James M. Skibo & Gary M. Feinman) 159-170 (University of Utah Press, 1999).

4 Clark, J. E. & Cheetham, D. in *Archaeology of tribal societies Archaeological Series, Vol. 15* (ed W. A. Parkinson) 278-339 (International Monograph in Prehistory, 2002).

5 Coe, M. D. & Diehl, R. A. *In the land of the Olmec*. (University of Texas Press, 1980).

6 Inomata, T. *et al.* Monumental architecture at Aguada Fénix and the rise of Maya civilization. *Nature* **582**, 530-533, doi:doi.org/10.1038/s41586-020-2343-4 (2020).

7 Rands, R. L. in *Palenque: recent investigations at the Classic Maya center* (ed Damien B. Marken) 25-56 (AltaMira, 2007).

8 Rands, R. L. in *Origins of Maya civilization* (ed Richard E. W. Adams) 159-180 (University of New Mexico Press, 1977).

9 Pope, K. O. *et al.* Origin and environmental setting of ancient agriculture in the lowlands of Mesoamerica. *Science* **292**, 1370-1372 (2001).

10 Chisholm, B. S. & Blake, M. in *Histories of maize: multidisciplinary approaches to the prehistory, linguistics, biogeography, domestication, and evolution of maize* (eds John E. Staller, Robert H. Tykot, & Bruce F. Benz) 161-172 (Academic Press, 2006).

11 Blake, M., Clark, J. E., Voorhies, B., Love, M. W. & Chisholm, B. S. Prehistoric subsistence in the Soconusco region. *Current anthropology* **33**, 83-94 (1992).

12 Clark, J. E., Pye, M. E. & Gosser, D. C. in *Archaeology, art, and ethnogenesis in Mesoamerican prehistory: papers in honor of Gareth W. Lowe Papers of the New World Archaeological Foundation, Vol. 68* (eds Lynneth S. Lowe & Mary E. Pye) 23-42 (Brigham Young University, 2007).

13 Cyphers, A. & Zurita-Noguera, J. in *Early New World Monumentality* (eds Richard L. Burger & Robert M. Rosenswig) 138-173 (University Press of Florida, 2012).

14 Killion, T. W. Nonagricultural cultivation and social complexity: the Olmec, their ancestors, and Mexico's southern Gulf Coast lowlands. *Current Anthropology* **54**, 569-606 (2013).

15 Rosenswig, R. M., VanDerwarker, A. M., Culleton, B. J. & Kennett, D. J. Is it agriculture yet? Intensified maize-use at 1000 cal BC in the Soconusco and Mesoamerica. *Journal of Anthropological Archaeology* **40**, 89-108 (2015).

16 Rosenswig, R. M. in *Early Mesoamerican social transformations: Archaic and Formative lifeways in the Soconusco region* (ed Richard G. Lesure) 242-271 (University of California Press, 2011).

17 VanDerwarker, A. M. *Farming, hunting, and fishing in the Olmec world*. (University of Texas Press, 2006).

18 Kennett, D. J. *et al.* High-precision chronology for Central American maize diversification from El Gigante rockshelter, Honduras. *Proceedings of the National Academy of Sciences of the United States of America* **114**, 9026-9031, doi:10.1073/pnas.1705052114 [doi] (2017).

19 Kennett, D. J. *et al.* Early isotopic evidence for maize as a staple grain in the Americas. *Science Advances* **6**, eaba3245, doi:10.1126/sciadv.aba3245 (2020).

20 Inomata, T. *et al.* Development of sedentary communities in the Maya lowlands: coexisting mobile groups and public ceremonies at Ceibal, Guatemala. *Proceedings of the National Academy of Sciences of the United States of America* **112**, 4268-4273, doi:10.1073/pnas.1501212112 [doi] (2015).

21 Lohse, J. C. Archaic origins of the lowland Maya. *Latin American Antiquity* **21**, 312-352 (2010).

22 Scherer, A. K. Bioarchaeology and the skeletons of the pre-Columbian Maya. *Journal of archaeological research* **25**, 133-184 (2017).

23 Tykot, R. H., van der Merwe, N. J. & Hammond, N. in *Archaeological chemistry: organic, inorganic, and biochemical analysis ACS Symposium Series 625* (ed M. V. Orna) 355-365 (American Chemical Society, 1996).

24 White, C. D. Gendered food behaviour among the Maya: time, place, status and ritual. *Journal of Social Archaeology* **5**, 356-382 (2005).

25 Wright, L. E. *Diet, health, and status among the Pasión Maya: a reappraisal of the collapse*. 1 edn, (Vanderbilt University Press, 2006).

26 Rust, W. F. *A settlement survey of La Venta, Tabasco, Mexico* Ph.D. thesis, University of Pennsylvania, (2008).

27 González Lauck, R. B. in *The place of stone monuments: context, use, and meaning in Mesoamerica's Preclassic tradition* (eds Julia Guernsey, John E. Clark, & Bábara Arroyo) 177-205 (Dumbarton Oaks Research Library and Collection, 2010).

28 Cyphers, A. in *The origins of Maya states* (eds Loa P. Traxler & Robert J. Sharer) 83-122 (University of Pennsylvania Museum of Archaeology and Anthropology, 2016).

29 Pool, C. A. *Olmec archaeology and early Mesoamerica*. (Cambridge University Press, 2007).

30 Doering, T. F. *An unexplored realm in the heartland of the southern Gulf Olmec: investigations at El Marquesillo, Veracruz, Mexico*, University of South Florida, (2007).

31 Santley, R. S. *The prehistory of the Tuxtlas*. (University of New Mexico Press, 2007).

32 Liendo Stuardo, R. *B'aakal: arqueología de la región de Palenque, Chiapas, México: temporadas 1996-2006*. (Archaeopress, 2011).

33 Rands, R. L. in *Mesoamerican archaeology: new approaches* (ed Norman Hammond) 51-76 (University of Texas Press, 1974).

34 Vargas Pacheco, E. *Itzamkanac, El Tigre, Campeche: exploración, consolidación y análisis de los materiales de la Estructura 1*. (Universidad Nacional Autónoma de México, 2013).

35 Matheny, R. T. *The ceramics of Aguacatal, Campeche, Mexico*. (Brigham Young University, 1970).

36 Bachand, B. R. & Lowe, L. S. in *Arqueología reciente de Chiapas: contribuciones del encuentro celebrado en el 60º aniversario de la Fundación Arqueológica Nuevo Mundo Papers of the New World Archaeological Foundation No. 72* (eds Lynneth S. Lowe & Mary E. Pye) 45-68 (Brigham Young University, 2012).

37 Lowe, G. W. in *The origins of Maya civilization* (ed Richard E. W. Adams) 197-248 (University of New Mexico Press, 1977).

38 Lowe, G. W. in *The Olmec and their neighbors* (eds Michael D. Coe & David Grove) 231-256 (Dumbarton Oaks Research Library and Collection, 1981).

39 Miller, D. E. *Excavations at La Libertad, a Middle Formative ceremonial center in Chiapas, Mexico*. (Brigham Young University, 2014).

40 Clark, J. E. in *The origins of Maya states* (eds Loa P. Traxler & Robert J. Sharer) 123-224 (University of Pennsylvania Museum of Archaeology and Anthropology, 2016).

41 Clark, J. E. & Hansen, R. D. in *Royal courts of the ancient Maya, Volume 2: data and case studies* (eds Takeshi Inomata & Stephen D. Houston) 1-45 (Westview Press, 2001).

42 Hodgson, J. G., Clark, J. G. & Gallaga Murrieta, E. Ojo de Agua Monument 3: a new Olmec-style sculpture from Ojo de Agua, Chiapas, Mexico. *Mexicon* **32**, 139-144 (2010).

43 Love, M. & Guernsey, J. in *Early Mesoamerican social transformations: Archaic and Formative lifeways in the Soconusco region* (ed Richard G. Lesure) 170-188 (University of California Press, 2011).

44 Inomata, T. *et al.* High-precision radiocarbon dating of political collapse and dynastic origins at the Maya site of Ceibal, Guatemala. *Proceedings of the National Academy of Sciences of the United States of America* **114**, 1293-1298 (2017).

45 Inomata, T., Triadan, D., Aoyama, K., Castillo, V. & Yonenobu, H. Early ceremonial constructions at Ceibal, Guatemala, and the origins of lowland Maya civilization. *Science* **340**, 467-471, doi:10.1126/science.1234493 (2013).

46 Reimer, P. J. *et al.* The IntCal20 Northern Hemisphere radiocarbon age calibration curve (0–55 cal kBP). *Radiocarbon*, 1-33 (2020).

47 OxCal 4.4 (http://c14.arch.ox.ac.uk/, 2020).

48 Bayliss, A. Rolling out revolution: using radiocarbon dating in archaeology. *Radiocarbon* **51**, 123-147 (2009).

49 Bronk Ramsey, C. Bayesian analysis of radiocarbon dates. *Radiocarbon* **51**, 337-360 (2009).

50 Bronk Ramsey, C. Analysis of chronological information and radiocarbon calibration: the program OxCal. *Archaeological Computing Newsletter* **41**, 11-16 (1994).

51 Buck, C. E., Cavanagh, W. G. & Litton, C. D. *Bayesian approach to interpreting archaeological data*. (Wiley, 1996).

52 Inomata, T., Ortiz, R., Arroyo, B. & Robinson, E. J. Chronological revision of Preclassic Kaminaljuyú, Guatemala: implications for social processes in the Southern Maya area. *Latin American Antiquity* **25**, 377-408 (2014).

53 Bronk Ramsey, C. Dealing with outliers and offsets in radiocarbon dating. *Radiocarbon* **51**, 1023-1045 (2009).

54 Dee, M. & Bronk Ramsey, C. High-precision Bayesian modeling of samples susceptible to inbuilt age. *Radiocarbon* **56** (2013).

55 Bronk Ramsey, C. Radiocarbon calibration and analysis of stratigraphy: the OxCal program. *Radiocarbon* **37**, 425-430 (1995).